The Astrophysical Journal, 574:590–598, 2002 August 1

EARLY ENRICHMENT OF THE INTERGALACTIC MEDIUM AND ITS FEEDBACK ON GALAXY FORMATION

Evan Scannapieco,[1] Andrea Ferrara,[1] and Piero Madau[1,2]
Received 2002 January 25; accepted 2002 April 8

ABSTRACT

Supernova-driven outflows from early galaxies may have had a large impact on the kinetic and chemical properties of the intergalactic medium (IGM). We use three-dimensional Monte Carlo cosmological realizations of a simple linear peaks model to track the time evolution of such metal-enriched outflows and their feedback on galaxy formation. We find that at most 30% of the IGM by volume is enriched to values above $10^{-3}\ Z_\odot$ in models that include only objects that cool by atomic transitions. The majority of enrichment occurs relatively early ($5 \lesssim z \lesssim 12$) and leads to a mass-averaged cosmological metallicity between 10^{-3} and $10^{-1.5}\ Z_\odot$. The inclusion of Population III objects that cool through H_2 line emission has only a minor impact on these results: increasing the mean metallicity and filling factor by at most a factor of 1.4 and moving the dawn of the enrichment epoch to $z \approx 14$ at the earliest. Thus, enrichment by outflowing galaxies is likely to have been incomplete and inhomogeneous, biased to the areas near the starbursting galaxies themselves. Models with a 10% star formation efficiency can satisfactorily reproduce the nearly constant ($2 \leq z \leq 5$, $Z \approx 3.5 \times 10^{-4}\ Z_\odot$) metallicity of the low column density Lyα forest derived by Songaila in 2001, an effect of the decreasing efficiency of metal loss from larger galaxies. Finally, we show that IGM enrichment is intimately tied to the ram-pressure stripping of baryons from neighboring perturbations. This results in the suppression of at least 20% of the dwarf galaxies in the mass range $\sim 3 \times 10^8$–$3 \times 10^9\ M_\odot$ in all models with filling factors greater than 2% and an overall suppression of $\sim$50% of dwarf galaxies in the most observationally favored model.

Subject headings: galaxies: evolution — galaxies: interactions — intergalactic medium — large-scale structure of universe

1. INTRODUCTION

Recent quasar (QSO) absorption-line observations have shown that the intergalactic medium (IGM) is polluted with heavy elements at intermediate redshifts (Songaila & Cowie 1996). From such measurements of column density ratios $N_{\rm C\,IV}/N_{\rm H\,I}$, Hellsten et al. (1997) and Rauch, Haehnelt, & Steinmetz (1997) concluded that typically $[{\rm C/H}] \simeq -2.5$ at $z \simeq 3$, with an order of magnitude dispersion about this mean value.[3] These values, however, refer to overdense regions of the universe, traced by Lyα clouds with column densities in excess of $\log N_{\rm H\,I} = 14.5$.

The presence of metals has more recently been assessed in clouds in which $\log N_{\rm H\,I} < 14.0$, as reviewed by Pettini et al. (2000). At these low optical depths, statistical techniques to extend the search for highly ionized species such as C IV and O VI must be applied. The results show that (1) unrecognized weak C IV systems must be present in order to reproduce the full C IV optical depth (Ellison et al. 2000) and (2) that metals, as traced by O VI, are present in a gas with a density lower than that of the mean IGM (Schaye et al. 2000). Very recently, Songaila (2001) has been able to trace the IGM metallicity evolution in systems with $\log N_{\rm C\,IV} > 12$ and conclude that a minimum metallicity $Z \approx 3.5 \times 10^{-4}\ Z_\odot$ is already in place at $z = 5$.

Although these techniques help to extend QSO absorption studies to underdense regions of the IGM, present observations are only able to place a lower limit on the total volume filling factor of metals. Current measurements, combined with numerical simulations, indicate that metals associated with $\log N_{\rm H\,I} \lesssim 14.2$ filaments fill $\gtrsim 3\%$ of intergalactic space, including areas far away from the high overdensity peaks where galaxies form (Madau, Ferrara, & Rees 2001, hereafter MFR01). This suggests that metal pollution occurred relatively early, resulting in a more uniform distribution and enriching vast regions of intergalactic space. This allows the Lyα forest to be hydrodynamically "cold" at low redshifts, as intergalactic baryons have time to relax again under the influence of dark matter gravity. Note that the presence of high-redshift metals is of great observational importance, as the measurement of metal lines in $z \gtrsim 6$ quasars may also serve as a probe of reionization (Oh 2002).

These observations prompted MFR01 to suggest high-redshift ($z \approx 10$) galaxy outflows as a mechanism for IGM enrichment. This study could not determine the metal filling factor produced in such a scenario, however, as it was focused on the evolution of typical objects at a single mass scale and formation redshift. Similar outflow models have been proposed by Nath & Chiba (1995) and Scannapieco & Broadhurst (2001, hereafter SB01), but primarily motivated by the chemical and thermal properties of the X-ray–emitting gas in galaxy clusters. While the latter of these studies included a range of galaxy masses and was able to make some estimates as to the total filling factor of metals, these results were fairly crude, as the study was focused on the properties of individual galaxies. Aguirre et al. (2001a, 2001b) studied IGM metal enrichment by superposing an outflow model on numerical simulations that did not include supernova-driven (SN-driven) winds, but were only able to constrain the contribution from late-forming ($z \lesssim 6$)

[1] Osservatorio Astrofisico di Arcetri, Largo E. Fermi 5, Florence I-50125, Italy.
[2] Department of Astronomy and Astrophysics, 1156 High Street, University of California, Santa Cruz, CA 95064.
[3] In the usual notation, $[{\rm C/H}] = \log({\rm C/H}) - \log({\rm C/H})_\odot$.

and relatively large ($M \gtrsim 10^{8.5}\ M_\odot$) objects. Cen & Ostriker (1999) studied metal enrichment in even lower resolution smoothed particle hydrodynamic (SPH) simulations with a dark matter particle mass of $8.6 \times 10^8\ M_\odot$. Gnedin & Ostriker (1997) studied the relationship between reionization and early metal enrichment in high-resolution simulations but did not adequately follow SN explosions. Finally, Thacker, Scannapieco, & Davis (2002) were able to estimate the filling factor of outflows at $z \geq 4$ purely in the context of high-resolution SPH simulations with a dark matter particle mass of $2.5 \times 10^6\ M_\odot$ but were not able to examine its dependence on model parameters because of the high computational cost of this approach.

Early-enrichment scenarios also have important implications for the thermal and velocity structure of the IGM, as first studied in Tegmark, Silk, & Evrard (1993) and Voit (1996) (see also Cen & Bryan 2001). The resulting feedback on galaxy formation was first examined in Scannapieco, Ferrara, & Broadhurst (2000), SB01, and Scannapieco, Thacker, & Davis (2001). The nature of this effect is twofold: an impinging wind may shock-heat the gas of a nearby perturbation to above the virial temperature, thereby mechanically evaporating the gas, or the gas may be accelerated to above the escape velocity and stripped from the perturbation entirely. The latter channel is considerably more effective, because shock-heated clouds that are too large to be stripped are able to radiatively cool within a sound crossing time, thus limiting evaporation. Note that this type of feedback is fundamentally different from the one commonly adopted in galaxy formation models, in which hot gas is produced by SNe in the parent galaxy.

In this paper we return to the issues of enrichment and feedback, adopting a more complete approach that combines the detailed modeling of a typical object, as in MFR01, with the more general spatially dependent modeling described in SB01. In this way, we are able to place constraints on the overall metal filling factor produced as well as investigate the link between cosmic metal enrichment and the feedback from outflows on galaxy formation.

The structure of the paper is as follows. In §§ 2 and 3 we describe our semianalytical simulations of galaxy formation with feedback and IGM enrichment. In § 4 we summarize the results of these simulations and the constraints they place on the fraction of the universe impacted by outflows; conclusions are given in § 5.

2. A LINEAR PEAKS MODEL OF GALAXY FORMATION

In order to determine the distribution of outflows as a function of cosmic time, we use the linear peaks model described in detail in SB01. Note that it is important not only to have a measure of the overall number density of such objects but also of their spatial distribution, as high-redshift galaxies are expected to be highly clustered from both theory (e.g., Kaiser 1984) and observations (Giavalisco et al. 1998).

Using a standard fit to the cold dark matter (CDM) power spectrum (Bardeen et al. 1986), we construct a 256^3 linear density field spanning a $(4\ h^{-1}\ \mathrm{Mpc})^3$ cubic comoving volume, where h is the Hubble constant in units of 100 km $\mathrm{s}^{-1}\ \mathrm{Mpc}^{-1}$. Based mainly on the latest measurements of cosmic microwave background (CMB) anisotropies (e.g., Balbi et al. 2000; Netterfield et al. 2001; Pryke et al. 2002) and the abundance of galaxy clusters (Viana & Liddle 1996), we focus our attention on a cosmological model with parameters $h = 0.65$, $\Omega_m = 0.35$, $\Omega_\Lambda = 0.65$, $\Omega_b = 0.05$, $\sigma_8 = 0.87$, and $n = 1$, where Ω_m, Ω_Λ, and Ω_b are the total matter, vacuum, and baryonic densities in units of the critical density, σ_8 is the mass variance of linear fluctuations on the $8\ h^{-1}$ Mpc scale, and n is the tilt of the primordial power spectrum.

This linear density field is convolved with spherical "top-hat" window functions corresponding to nine different total masses, spaced in equal logarithmic intervals from 3.0×10^7 to $4.3 \times 10^{11}\ M_\odot$ and spanning the interesting range from objects that lie close to the lower limit set by photoionization and molecular cooling (e.g., Barkana & Loeb 1999; Ciardi, Ferrara, & Abel 2000a) to the most massive galaxies that host outflows. We assume that the formation of Population III (Pop III) objects, defined as halos with virial temperatures below 10^4 K, is completely suppressed by photodissociation of hydrogen molecules by UV radiation produced by nearby objects, and we study the impact of this assumption in further detail below.

Using the elliptical-collapse model of Sheth, Mo, & Tormen (2001), we identify all "virialized" peaks in the overdensity field, arrange them in order of decreasing collapse redshift, and exclude all unphysical objects collapsing within more massive, already virialized halos. After collapse, we account for the finite gas cooling time using a simple inside-out collapse model (White & Frenk 1991; Somerville 1997). The cooling gas initially relaxes to an isothermal distribution at the virial temperature T_{vir} in a Navarro, Frenk, & White (1997, hereafter NFW) dark matter halo with concentration parameter $c = 5$ and with a uniform metallicity Z calculated as described in the next section. In this model, the gas within a radius r_{cool} cools because of radiative losses that account for metallicity as tabulated by Sutherland & Dopita (1993), and the gas outside this radius stays at the virial temperature of the halo, with r_{cool} moving outward with time. This model is described in further detail in SB01.

When the total mass contained within r_{cool} equals the object's baryonic mass, a new galaxy is assumed to form with a gas mass $M_b = (\Omega_b/\Omega_m)M$. In the smaller halos at high redshift having $\log T_{\mathrm{vir}} < 5.7$ (i.e., masses $M < 2 \times 10^{10}[(1+z)/10]^{-3/2}\ M_\odot$), rapid cooling by atomic hydrogen and helium occurs on timescales much shorter than the gas free-fall time, and infalling gas collapses to the center at the free-fall rate rather than coming to hydrostatic equilibrium (MFR01). The supply of cold gas for star formation is then limited only by the infall rate.

We assume a Salpeter initial mass function with upper and lower mass cutoffs equal to $M_u = 120\ M_\odot$ and $M_l = 0.1\ M_\odot$, respectively. In this case, one SN occurs for every $\nu^{-1} \approx 136\ M_\odot$ of stars formed, releasing an energy of $E_0 = 10^{51}$ ergs. This mechanical energy is injected by SNe after a few $\times\ 10^7$ yr: at this stage, SN-driven bubbles propagate into the halo, quenching further star formation, and the conversion of cold gas into stars is limited by the increasing fractional volume occupied by SN remnants. To be conservative, we do not consider the possibility that very massive ($\approx 300\ M_\odot$), metal-free stars might contribute to both metallicity and energy input. Their effects have been discussed in detail by Schneider et al. (2002a) and Schneider, Guetta, & Ferrara (2002b), to which we refer the reader for an extensive description.

Before SN feedback occurs, some fraction f_* of the gas will be able to cool, fragment, and form stars. As our formalism does not include local feedback effects, this star formation efficiency must be considered as a free parameter of the model. Finally, a fraction f_w of this energy will be channeled at a constant rate into a galaxy outflow over a timescale span of $t_{OB} = 33$ Myr, ejecting gas into the IGM.

As we show below, the most efficient IGM polluters are objects with masses of a few $\times 10^8\ M_\odot$, for which the fraction of gas that can cool in a free-fall time is essentially unity (MFR01). Hence, this gas is readily available to be transformed into stars on short timescales. This justifies the prompt star formation (starburst mode) approximation we have adopted, which therefore should be appropriate to the aims of this study.

3. MODELING GALAXY OUTFLOWS

The outflows are modeled as spherical shells using a method that is based on the approach described in SB01, but with several important refinements taken from MFR01, Ferrara, Pettini, & Shchekinov (2000), and Mori, Ferrara, & Madau (2001, hereafter MFM01). An outflow is driven out of the galaxy by internal pressure and decelerated by inertia and the gravitational pull of the dark matter halo, both estimated in the thin-shell approximation (Ostriker & McKee 1988; Tegmark et al. 1993).

The expansion of the shell, whose radius is denoted by R_s, is driven by the internal energy E_b of the hot bubble gas. The pressure of such a gas (with adiabatic index $\gamma = 5/3$) is therefore $P_b = E_b/2\pi R_s^3$. Momentum and energy conservation yield the relevant evolutionary equations,

$$\dot{R}_s = \frac{3(P_b - P)}{\rho R_s} - \frac{3}{R_s}(\dot{R}_s - HR_s)^2 - \Omega_m \frac{H^2 R_s}{2} - g_s\ ,$$
$$\dot{E}_b = L(t) - 4\pi R_s^2 \dot{R}_s P_b - L_c\ , \qquad (1)$$

where the dots represent time derivatives, the subscripts s and b indicate shell and bubble quantities, respectively, $g_s \equiv GM(R_s)/R_s^2$, and ρ is the density of the ambient medium, taken to be the halo gas density within the virial radius and the mean IGM background density outside the virial radius. These equations reduce to those given in MFR01 in the regime in which the Hubble expansion is negligible and reduce to those given in SB01 if the NFW profile is replaced by a point mass and external pressure is neglected.

The cooling rate L_c is assumed here to be dominated by inverse Compton cooling off of CMB photons (Ikeuchi & Ostriker 1986), as gas radiative processes are much less efficient in the low-density $10^5\ \mathrm{K} \le T \le 10^8$ K gas that drives the outflows. This approximation is especially appropriate as the combined cooling processes produce variations of less than a few percent on the final size of the bubble (see Fig. 6 of MFR01).

The mechanical luminosity of SNe is given by

$$L(t) = (f_w E_0)\frac{\nu M_*}{t_{OB}}\Theta(t_{OB} - t)$$
$$= 8.26 \times 10^{33}\Theta(t_{OB} - t)\left(\frac{\Omega_b}{\Omega_m}\right) f_w f_* M\ \mathrm{ergs\ s^{-1}}\ . \qquad (2)$$

This assumption of a constant luminosity over the burst is most accurate for the larger galaxies in our simulations, in which the stochastic variations of $L(t)$ become smaller due to the larger number of SNe. We constrain f_w by combining the overall efficiency of 30% derived for the $2 \times 10^8\ M_\odot$ object simulated by MFM01 with the mass scaling derived in Ferrara et al. (2000), which was obtained by determining the fraction of starburst sites that can produce a blowout in a galaxy of a given mass. Thus, we choose $f_w(M) = 0.3\delta_B(M)/\delta_B(M = 2 \times 10^8\ M_\odot)$, where

$$\delta_B(M) = \begin{cases} 1.0\ , & \tilde{N}_t \le 1\ , \\ 1.0 - 0.165\ln\left(\tilde{N}_t^{-1}\right)\ , & 1 \le \tilde{N}_t \le 100\ , \\ [1.0 - 0.165\ln(100)]100\tilde{N}_t^{-1}\ , & 100 \le \tilde{N}_t\ , \end{cases} \qquad (3)$$

where $\tilde{N}_t \equiv 1.7 \times 10^{-7}(\Omega_b/\Omega_m)M/M_\odot$ is a dimensionless parameter that scales according to the overall number of SNe produced in a starburst, divided by the efficiency f_*.

Within the virial radius, a fixed fraction $f_m = 0.5$ of the gas is swept into the shell, a value taken from the numerical simulations described in MFM01. In those experiments it is seen that after blowout, half of the initial mass contained in the virial radius recollapses to the center as a result of the multiple shell-shell interactions leading to the formation of cold sheets. In this case, the halo gas is assumed to virialize to an isothermal distribution and settle down to a density profile

$$\ln\rho(r) = \ln(f_m\rho_0) - \frac{\mu m_p}{2kT_{\mathrm{vir}}}\left[v_e^2(0) - v_e^2(r)\right] \qquad (4)$$

(Makino, Sasaki, & Suto 1998), where the central, preburst gas density ρ_0 is determined by the condition that the total baryonic mass fraction within the virial radius is equal to the cosmic average, yielding $\rho_0 = 11,052\rho_{\mathrm{crit}}\Omega_b$.

Outside the virial radius, the shells expand into the Hubble flow, sweeping up all of the baryons in their path. Finally, when outflows slow down to the point that they are no longer supersonic, our approximations break down, and the shell is possibly fragmented by random motions. At this point, we let the bubble expand with the Hubble flow.

To calculate the cooling time of forming galaxies (see § 2), we use a simple estimate of the metallicity of collapsed halos. The metals in each outflow are assumed to be evenly distributed within its radius, adopting an average yield from each SN of $2\ M_\odot$ (e.g., Nagataki & Sato 1998), half of which is deposited in the outflow and half of which remains in the galaxy. Each collapsing object is then assigned a mass in metals M_Z, taken to be zero initially and modified by each outflow passing within its collapse radius r_{coll}. We assume that the fraction of metals that falls into the collapsing halo from a given outflow is equal to the volume fraction of the outflowing bubble that falls within the collapsing sphere. In this case, for each overlapping bubble, M_Z is updated to

$$M_Z \rightarrow M_Z + \frac{V_{\mathrm{overlap}}}{(4\pi/3)r_{\mathrm{coll}}^3} M_Z^{\mathrm{blast}}\ , \qquad (5)$$

where V_{overlap} is the volume of intersection between the outflow and the collapsing sphere. By dividing this mass by the total baryonic mass of the galaxy, we can compute the initial metallicity of the object and thus the delay between collapse and star formation due to cooling. Note, however, that this cooling time is only significant at the highest mass scales, $\gtrsim 10^{10}\ M_\odot$.

Our model is also able to account for the inhibition of surrounding low-mass galaxy formation (i.e., negative feedback). Scannapieco et al. (2000) showed that the most important such mechanism is "baryonic stripping," whereby high-redshift galaxy outflows strip the gas out of nearby overdense regions that would have otherwise become low-mass galaxies. Whenever a shock moves through the center of an overdense region that has not yet virialized, we apply a simple check to determine if such stripping has occurred.

In each case, we estimate the comoving radius of the overdense region as $r_m(1+\delta_{\rm NL})^{-1/3}$, where $\delta_{\rm NL}$ is the nonlinear overdensity of the region, which is estimated from the spherical-collapse model as

$$1+\delta_{\rm NL}=\frac{9}{2}\frac{(\theta-\sin\theta)^2}{(1-\cos\theta)^3}\ , \tag{6}$$

where the collapse parameter θ is given by $(\theta-\sin\theta)^{2/3}\pi^{-2/3}=D(z_{\rm cross})/D(z_c)$, where $z_{\rm cross}$ is the redshift at which the shock moves through the center of the objects, z_c is its collapse redshift, computed from the model of Sheth, Mo, & Tormen (2001), and $D(z)$ is the linear growth factor as a function of redshift. We then inhibit galaxy formation if the shock has sufficient momentum to accelerate the gas to its escape velocity,

$$\omega M_s\dot{R}_s\geq M_p v_e\ , \tag{7}$$

where ω is the solid angle of the shell subtended by the perturbation, M_s is the baryonic mass swept up by the shock, including both the IGM and gas ejected from the host objects, v_s is the velocity of the shock, and M_p and $v_e=2GM_p(1+\delta_{\rm NL})^{1/3}/r_{M_p}$ are the gas mass and escape velocity of the perturbation.

In SB01 we simply estimated the filling factor of outflows by summing over the volumes contained within all galaxy outflows, regardless of their mass scales or spatial distribution. As this investigation is focused on determining the overall state of the IGM, here we adopt a more accurate approach in which we construct a 256^3 grid, search through the expanding bubbles, and count all grid points within them as a function of redshift.

Our approach also differs from that in SB01 in our treatment of outflows expanding from host galaxies that merge. While our previous estimates only counted outflows from unmerged host galaxies, in this work we instead take the wind to remain fixed at the comoving radius found at the time of the merger. This is because, while it is clear that our approximation of a spherical pressure-driven wind is broken when a merging galaxy passes through this shell, it is unlikely that such a merger would be able to absorb all the gas ejected, somehow erasing the wind from existence.

It is important to point out that although our estimate of the filling factor takes into account the spatial orientation of the bubbles, our formalism fails to capture the interaction between expanding shock fronts. In the case in which two outflows are expanding in opposite directions, our approach allows them to pass through each other unhindered, leading to a slight overestimate of the volume impacted. Similarly, in the case in which an outflow expands into a bubble evacuated by a previous wind, it is nevertheless modeled as if it were expanding into the Hubble flow, leading to a slight underestimate.

4. RESULTS

4.1. *Cosmic Metal Filling Factor*

In the left panels of Figure 1, we show the derived filling factor of outflows. Here, the bend at $z\approx 13$ is due to our finite mass resolution. At this redshift, the smallest mass scale drops below the virial temperature limit of 10^4 K, causing the effective resolution of the simulation to jump to the next mass scale. In reality, objects between these two mass scales are formed, and the metals from these objects would smooth the evolution of the filling factor. Finally, because our method becomes inaccurate when perturbations are overly nonlinear, we restrict this figure to redshifts above 3.

The parameters in these models are $f_*=0.5$, 0.1, and 0.01, $f_w(M)=0.3\delta_B(M)/\delta_B(2\times10^8\ M_\odot)$ with δ_B as in equation (3), $\nu^{-1}=136\ M_\odot$, $t_{OB}=33$ Myr, and $f_m=0.5$. The first three of these parameters appear in combination both in the expression for the overall strength of the winds ($\propto f_* f_w \nu$), and the metallicity ($\propto f_*\nu$). On the other hand, t_{OB} has almost no effect on our results, as the relevant times for star formation are small compared to structure formation timescales. Thus, we can provide a conservative estimate of the model uncertainties introduced by these parameters by simply considering a wide range of star-formation efficiencies and applying a linear shift in the final metallicity to estimate the effect of varying f_w. Finally, while the mass-loading parameter f_m has little effect on the overall filling factor, it is important for galaxy feedback, and we consider its impact in detail in § 4.3.

The most obvious, yet perhaps most important feature of Figure 1 is that the filling factor is always substantially less than unity, ranging from 3% to 30% at $z=3$. Note that these values are consistent with the 20% enrichment at $z=4$ found in numerical simulations by Thacker et al. (2002), using a model similar to our $f_*=0.1$ case. The fact that IGM enrichment is inhomogeneous even in the maximal case, in which 50% of all baryons in collapsed objects are taken to form stars, however, leads us to an important conclusion: starburst-driven outflows, while an effective source of metals in overdense regions (SB01), are not able to enrich the IGM in its entirety. This is true even in the ΛCDM model considered in our simulations, in which dwarf galaxies are formed at very high redshifts and the baryonic/dark matter ratio is relatively high, resulting in a large number of stars.

The details of our results depend sensitively on the minimum mass scale of the galaxies in our simulation, however, which is set by our minimum virial temperature of 10^4 K. In the central panel of this figure, we plot a series of models in which no feedback as per equation (7) is imposed, but instead we allow outflows only from objects above a fixed mass scale. Both the redshift at which outflows begin to become important and their overall filling factor depend closely on this mass. Thus, while in the run with $f_*=0.1$ outflowing bubbles fill 1% of the volume at redshift $\lesssim 12$ and reach a final filling factor of 16%, excluding all objects with masses below $1.1\times10^9\ M_\odot$ shifts these values to $z\approx 8$ and 6%, respectively. Note that this lower resolution is similar to that adopted by Aguirre et al. (2001b) and approximately equal to the mass of a single dark matter particle in the simulations by Cen & Ostriker (1999).

In spite of the sensitivity of metal enrichment to low-mass objects, its overall dependence on baryonic-stripping feedback is weak, as can be seen by comparing the solid lines in

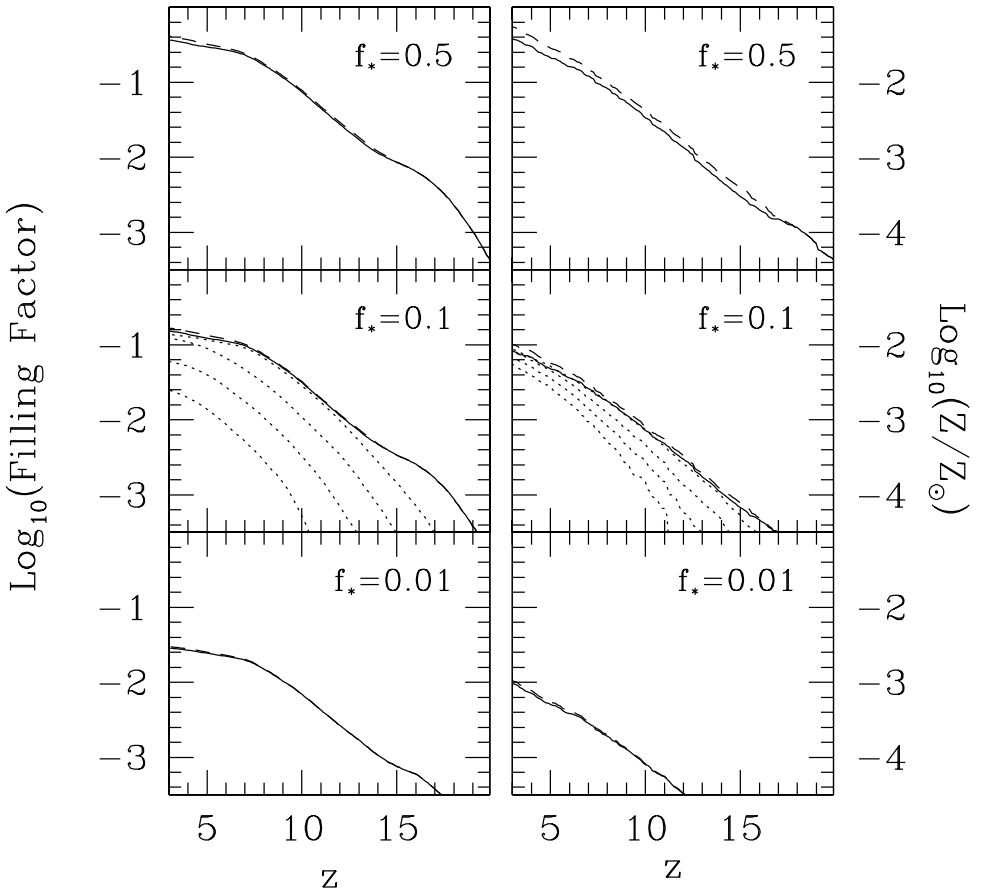

FIG. 1.—*Left*: Cosmic metal filling factor from galaxy outflows. In each panel, solid lines show the filling factor in runs with the inclusion of baryonic stripping feedback according to eq. (7), and dashed lines show the filling factor without. Each panel is labeled by the overall star formation coefficient f_*, and in the $f_* = 0.1$ case, the dotted lines represent models in which there is no feedback, but outflows are only generated by objects at or above a fixed mass limit. From top to bottom, these limits are 1.0×10^8, 3.3×10^8, 1.1×10^9, and 3.6×10^9 $M_\odot$. *Right*: Mass-averaged IGM metallicity as a function of redshift. Curves are as in the left panels.

which equation (7) has been imposed with the dashed lines in which such feedback from outflows is neglected. The shape and final value of the filling factor are extremely similar between such models for all values of f_*, becoming indistinguishable in many cases. This is because baryonic stripping can only occur in a perturbation that is sufficiently nearby and late-collapsing. Then the shock velocity $\dot{R}_s$ is large, and the overdense region occupies a large solid angle ω when the outflow reaches it. Thus, the perturbations succumbing to baryonic stripping correspond to late-forming galaxies in the most heavily populated regions of space, which have little effect on the overall filling factor.

The higher bias of suppressed objects can also be seen by comparing the evolution of the filling factor with the overall mass-averaged IGM metallicity, plotted in the right panels of Figure 1. In these panels, the differences between the models with and without suppression are much more pronounced. The difference is most apparent in the $f_* = 0.5$ case, in which the wind velocities are the highest, and thus the suppression of neighbors is most severe. In this case at $z = 3$, the overall metallicities differ by a factor of 1.5, while the difference in volume filling factor is less than a factor of 1.15.

Note that the mass-averaged metallicity scales almost linearly with f_*, as this parameter controls the number of stars formed in each galaxy and hence the number of SNe and mass of ejected metals. We find that at $z = 3$, $Z \approx 0.1 f_*$, where this relation depends on the assumed yield (2 $M_\odot$ per SN, half ejected), the gas-ejected fraction (50%), and the minimum mass scale in the simulation. This mass dependence, while sensitive, is more limited than that of the overall filling factor, as can be seen by comparing the $f_* = 0.1$ model with the series of models with a threshold mass imposed, plotted in the center right panel. Thus, the model with $T_{\rm vir} \geq 10^4$ K (*solid line*) and that with a fixed threshold of 1.1×10^9 $M_\odot$ have $z = 3$ metallicities of 0.010 and 0.007 $Z_\odot$, respectively.

In Figure 2 we examine the distribution of metals in more detail by computing the filling factor of gas above a fixed threshold metallicity. As the metallicities of individual outflows always exceed 10^{-3} $Z_\odot$ in all models, the filling factor at this threshold metallicity is indistinguishable from the total filling factor as shown in Figure 1.

Choosing a higher threshold value, however, leads to more model-dependent results. From this point of view, the $f_* = 0.5$ and 0.1 models are quite similar, and in both cases, approximately 50% of the enriched gas has a metallicity greater than 10^{-2} $Z_\odot$, 10% of the enriched gas exceeds 10^{-1} $Z_\odot$, and 1% of the enriched IGM exceeds solar metallicity. On the other hand, the distribution of metals is much more clumpy in the weak star formation ($f_* = 0.01$) case. Here, while about 50% of the enriched IGM exceeds 10^{-2}

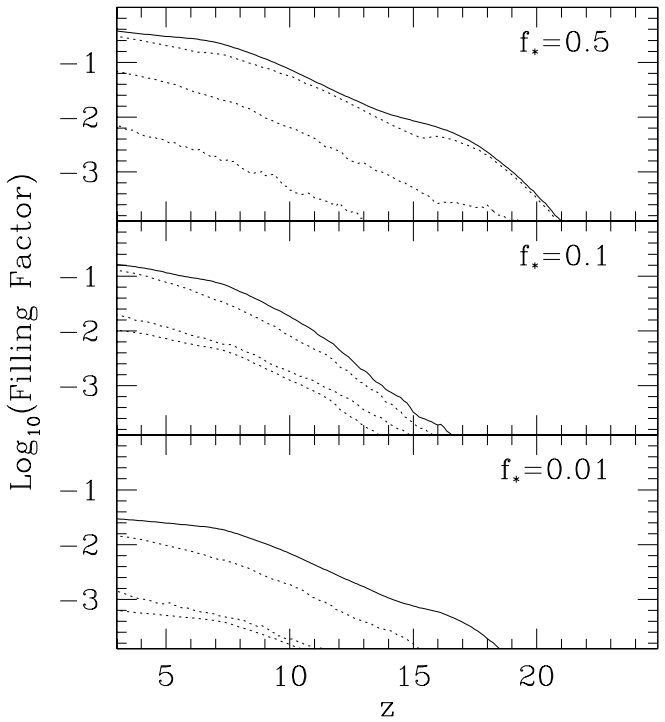

FIG. 2.—Cosmic metal filling factor from galaxy outflows, as a function of threshold metallicity. In each panel, the solid lines show the total filling factor of metals, which is indistinguishable from the filling factor of gas with $Z \geq 10^{-3}\ Z_{\odot}$. The dotted lines, from top to bottom, show the filling factor of gas enriched to values above 10^{-2}, 10^{-1}, and 1 $Z_{\odot}$, respectively.

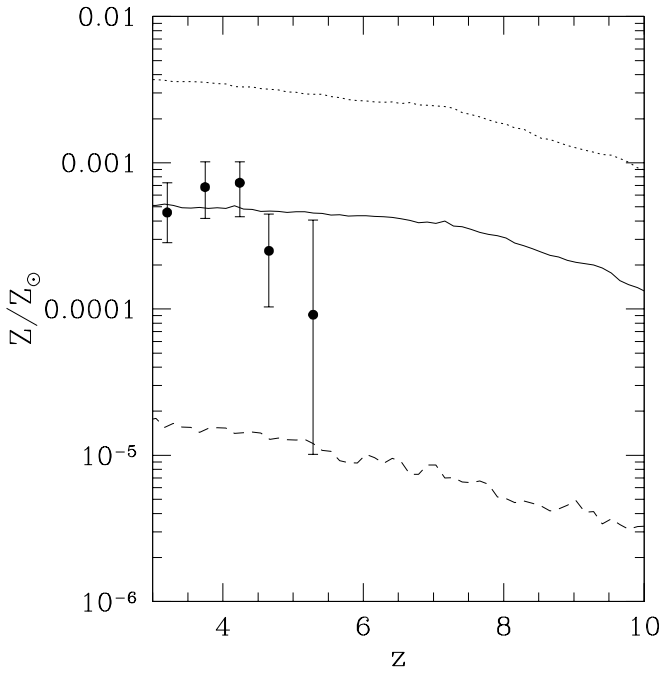

FIG. 3.—Metallicity evolution for low-density (10^{12} cm$^{-2} < N_{\rm H\,I} < 10^{15}$ cm^{-2}) IGM. Points are the data of Songaila (2001); dotted, solid, and dashed lines are the predicted values for $f_* = 0.5$, 0.1, and 0.01, respectively.

$Z_{\odot}$, the volume fraction of enriched gas with metallicities above 10^{-1} and 1 $Z_{\odot}$ are quite similar, with such high-metallicity gas occupying approximately 6% and 3% of the enriched volume, respectively.

Our estimates of the IGM metallicity invite comparison with that recently observed in the low column density Lyα forest. Songaila (2001) derived the redshift evolution of $\Omega_{\rm C\,IV}$ and $\Omega_{\rm Si\,IV}$ for a large number of systems (367 and 109 for C IV and Si IV, respectively) with H I column densities 10^{12} cm$^{-2} < N_{\rm H\,I} < 10^{15}$ cm^{-2}. The above quantities could then be translated, modulo the assumption of the ionization fraction of such species taken to be equal to 0.5, into a metallicity estimate. The resulting metallicity evolution is shown by the points in Figure 3, with the error bars corresponding to a 90% confidence limit. Songaila (2001) points out two striking features of IGM enrichment: (1) the existence of a minimum metallicity $Z \approx 10^{-3.45}\ Z_{\odot}$, already in place at $z = 5$, and (2) a constancy of metal abundances through the studied redshift range $z = 2$–5. A direct comparison of our simulations with these results is possible provided that we filter our metallicity estimates with the overdensities sampled by Songaila's experiment. Ricotti, Gnedin, & Shull (2000) showed that a clear correlation between H I column and gas overdensity exists, with $\rho_b/\overline{\rho}_b \simeq 0.8 N_{\rm H\,I,13}^{0.7}$; hence, the 10^{12} cm$^{-2} < N_{\rm H\,I} < 10^{15}$ cm^{-2} range can be translated into the overdensity range $0.16 \lesssim \rho_b/\overline{\rho}_b \lesssim 20$.

Adopting the smallest filter scale and associating linear and nonlinear overdensities according to equation (6), we have searched through our simulations and computed a mass-averaged metallicity of cells that are not surrounded by a collapsed perturbation and in which $0.8 \lesssim \rho_b/\overline{\rho}_b \lesssim 20$, roughly corresponding to QSO absorption systems with 10^{13} cm$^{-2} < N_{\rm H\,I} < 10^{15}$ cm^{-2}. We adopt this lower bound, as our mapping between linear and nonlinear overdensities becomes unreliable for smaller values of δ. These results are superposed on the data points in Figure 3 for the usual three values of f_*. Although no fitting parameter has been adjusted to produce these curves, the resemblance to the data, in terms of both amplitude and flat shape, is noticeable. It is only at redshifts above $z = 8$ that the curve starts to bend downward. The physical interpretation for the existence of this metallicity floor is simple: metal enrichment is dominated by low-mass (10^8–10^9 $M_{\odot}$) objects for which metal ejection/transport occurs with highest efficiency (see discussion in Ferrara, Pettini, & Shchekinov; eq. [3]). As the nonlinear mass scale increases, larger but intrinsically less efficient galaxies become the most numerous population. However, they contribute only marginally to metal enrichment of the Lyα forest as synthesized metals are predominantly trapped by their potential wells. This explains both the shape and amplitude of the data, provided $f_* \approx 0.1$, a value that is broadly consistent with other arguments based on cosmic star formation rates (Ciardi et al. 2000b; Thacker et al. 2002; Barkana 2002).

4.2. *Population III Objects*

In order to study the impact of Pop III objects on our results, we have conducted a number of comparison simulations in which we allow objects with virial temperatures less than 10^4 K to form, but with a lower overall star formation efficiency. In these cases, we took $f_{*\rm Pop\,III} = 0.1 f_*$ in objects with $T < 10^4$ K. This is physically motivated by the lower efficiency of molecular hydrogen cooling, which reduces the number of cooled baryons available to form stars. For each

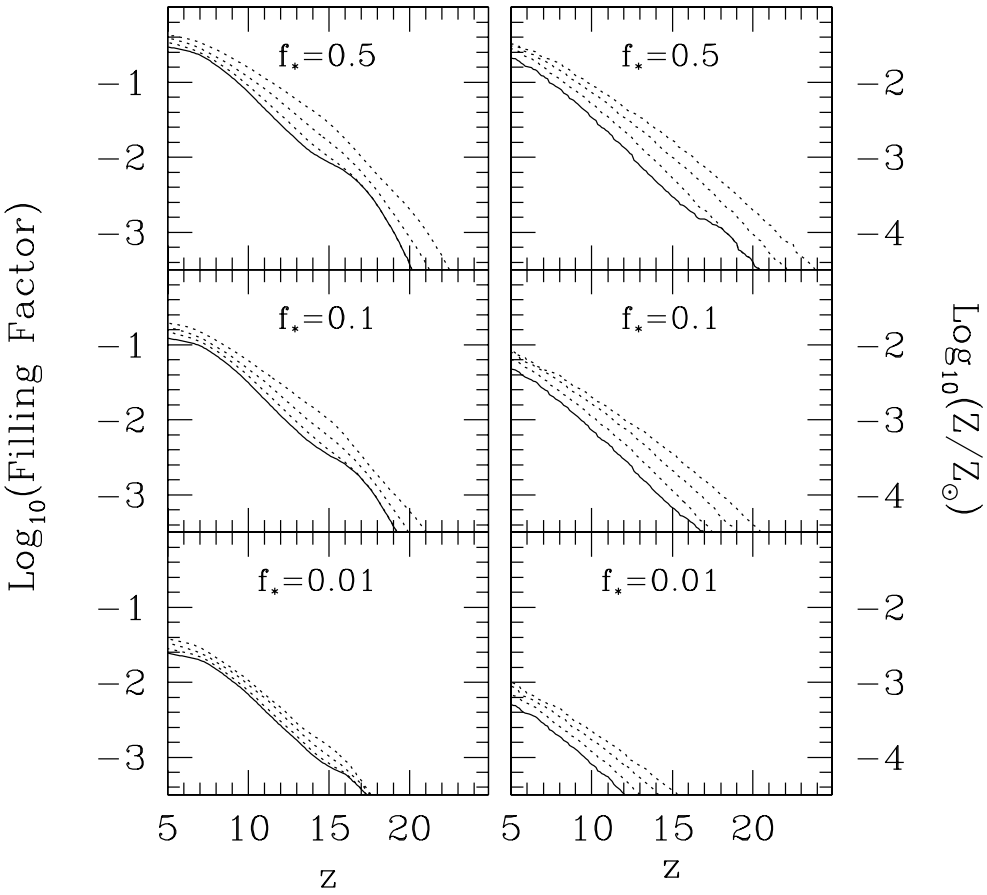

FIG. 4.—Impact of Pop III objects. In each panel, the solid lines show the filling factor and total metallicity in runs with a minimum mass scale of 3.0×10^7 $M_\odot$ and a minimum $T_{\rm vir} = 10^4$ K, as in Fig. 1. The dotted lines are taken from runs that include star formation in objects with $T_{\rm vir} < 10^4$ K, as described in the text. From top to bottom, the minimum mass scale in these simulations is 3.0×10^6, 1.0×10^7, and 3.0×10^7 $M_\odot$, corresponding to virial temperatures of 5000, 12,000, and 26,000 K at $z = 20$ and 2800, 6000, and 13,000 K at $z = 10$.

value of f_*, we conducted three such comparison runs: one with the same overall resolution as the fiducial case (a 4 h^{-1} Mpc comoving box with objects with nine mass scales ranging from 3.0×10^7 to 4.3×10^{11} $M_\odot$), one in a 2.75 h^{-1} Mpc comoving box with the nine mass scales now ranging from 1.0×10^8 to 1.3×10^{11} $M_\odot$, and one in a 1.75 h^{-1} Mpc comoving box with masses ranging from 3.0×10^6 to 4.3×10^{11} $M_\odot$. Note that in the last of these simulations, the smallest objects have virial temperatures $\leq$5000 K at redshifts below 20 and are thus not only well below the 10^4 K atomic cooling limit, but also below the 5000 K limit for "efficient" molecular cooling at which the cooling time exceeds the free-fall time (MFR01).

The filling factor and overall metallicities in the comparison runs are shown in Figure 4. Here we restrict our analysis to redshifts above 5, so that our linear approach remains accurate at the smallest mass scales. In this figure we see that even in the case with the highest resolution, Pop III objects are only able to increase the metal filling factor and metallicity of the IGM to values that are a factor of 1.4 times greater than those found in the standard runs. Similarly, these objects have only a small impact on the redshift at which outflows fill 1% of the volume, pushing this value from 12 to 14 in the $f_* = 0.1$ case. From this comparison, it is clear that while our results are sensitive to imposing a mass limit above $T_{\rm vir} = 10^4$ K, they are relatively insensitive to the inclusion of Pop III objects, which rely on H_2 line cooling for collapse.

4.3. *Feedback*

In Figure 5 we explore in greater detail the relationship between the cosmic filling factor and baryonic stripping. While the suppression of galaxy formation has little impact on the cosmic metal filling factor, these quantities are clearly related, as both are dependent on the number density and strength of galaxy outflows. In this plot we quantify baryonic stripping by counting all galaxies with masses above 3.2×10^8 $M_\odot$, excluding the objects at the smallest two mass scales, as at low redshifts their virial temperatures fall below the 10^4 K limit. In this case, the majority of suppressed objects are slightly larger dwarf galaxies with masses of a few $\times 10^9$ $M_\odot$ (SB01; Scannapieco et al. 2001).

In the top panel of this figure, we see that while the details of outflow generation and propagation introduce a large scatter, widespread IGM enrichment is accompanied by a significant level of baryonic stripping in all cases. Thus, even given the wide range of f_* values considered, all models and redshifts in which 2% of the IGM is enriched show a suppression of galaxies $\gtrsim$20%. In the $f_* = 0.1$ case, which is most consistent with QSO observations, approximately half

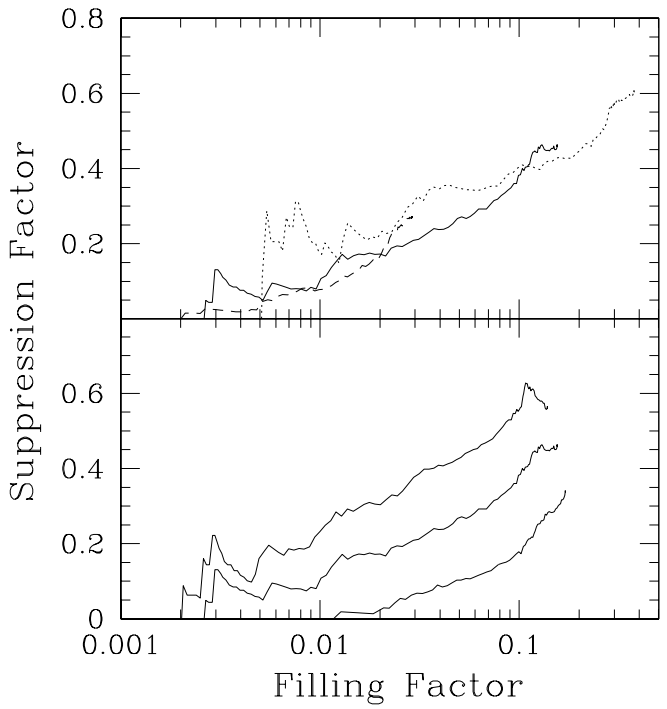

FIG. 5.—*Top*: Fraction of galaxies suppressed by baryonic stripping as a function of the overall metal filling factor. The dotted, solid, and dashed curves correspond to models in which f_* is set to 0.5, 0.1, and 0.01, respectively. *Bottom*: Impact of f_m on the suppression of galaxy formation. From top to bottom, $f_m = 1.0$, 0.5, and 0.25, with $f_* = 0.1$ in all cases.

of the objects with masses at or above $3.2 \times 10^8\ M_\odot$ are suppressed by this mechanism by $z = 3$.

These results are sensitive, however, to the mass-loading parameter f_m, as the suppression of galaxy formation is primarily due to the momentum carried by the winds (see, e.g., Scannapieco et al. 2000; Scannapieco et al. 2001), which scales as $E_b^{1/2} M_s^{1/2}$. Thus, increasing the fraction of gas swept into the shells increases galaxy suppression in models with the same kinetic energy input. In the bottom panel of Figure 5, we compare our fiducial $f_* = 0.1$, $f_m = 0.5$ model with an enhanced feedback model in which $f_m = 1.0$ (and with a depressed feedback model in which $f_m = 0.25$). Although changes in f_* result in a simultaneous increase of both the filling factor and suppression factor of dwarf galaxies, changing f_m shifts the suppression factor while having little effect on the overall filling factor. Thus, the filling factors in these models are all between 14% and 18%, while the fraction of suppressed dwarf galaxies varies from 35% to 60%.

As a general remark about this type of feedback, we note that the gas swept from the potential well is unlikely to be reaccreted by this object. Instead, this gas will be available to other collapsing objects, which therefore can be characterized by higher baryon-to–dark matter ratios. Clearly, in order to draw more quantitative conclusions, a dedicated hydrodynamical study of the details of baryonic stripping is required.

5. CONCLUSIONS

In this work we have studied the metal enrichment of the IGM by outflows in a ΛCDM model of structure formation and its feedback on the formation of galaxies. Adopting a linear peaks model of the spatial distribution of forming objects and a detailed one-dimensional model of wind propagation, we have determined the overall filling factor as a function of redshift and its relationship with the baryonic stripping of protogalaxies.

While the star formation efficiency of high-redshift galaxies is largely unknown, we are nevertheless able to place useful constraints on the filling factor, enrichment redshift, and overall mass-averaged metallicity in such models. Choosing a range of star formation efficiencies between $f_* = 0.50$ and 0.01, we find that at least 3% and at most 30% of the IGM is enriched to a level exceeding $10^{-3}\ Z_\odot$ by redshift $z = 3$. In all cases, the majority of this enrichment occurs relatively early, $5 \lesssim z \lesssim 12$, and leads to mass-averaged cosmic metallicities that range from 0.001 to 0.05 $Z_\odot$, for star formation efficiencies $0.01 < f_* < 0.5$, respectively. The mass-averaged metallicity scales roughly linearly with this quantity: $Z \approx 0.1 f_*\ Z_\odot$.

Our model can satisfactorily reproduce the constant ($Z \approx 3.5 \times 10^{-4}\ Z_\odot$) metal enrichment of the low column density Lyα forest up to $z = 5$ derived by Songaila (2001), which is likely to be caused by the decreasing efficiency of metal loss from larger galaxies. This comparison strongly favors star formation efficiencies in a narrow range around 10%, essentially excluding the $f_* = 0.5$ and 0.01 models. As the formation of stars in Pop III objects is relatively inefficient, the inclusion of these objects has only a secondary effect on our results: increasing the mass-averaged metallicity and filling factors by at most a factor of 1.4 and moving the dawn of the enrichment epoch to $z \approx 14$ at the earliest.

While all the models studied display suppression of galaxy formation due to outflows ram-pressure stripping the gas out of previrialized protogalaxies, this mechanism has only a minor impact on the overall filling factor, as it occurs only in the densest and most polluted regions of space. Nevertheless, after fixing f_m, a general relationship between the filling factor and the suppression factor of galaxies exists at all f_* values. All models and redshifts at which 2% of the IGM is enriched show a greater than 20% suppression of galaxies. In the case that is most consistent with QSO observations, in fact, half the galaxies are suppressed because of baryonic stripping. Thus, the relative quiescence of the Lyα forest at lower redshifts is likely to belie a violent epoch of early outflows and enrichment.

Support for this project was provided by NASA through ATP grant NAG 5-4236 and LTSA grant NAG 5-11513 and by a B. Rossi visiting fellowship at the Observatory of Arcetri (P. M.). E. S. was supported in part by an NSF MPS-DRF fellowship. A. F. and P. M. also acknowledge the support of the EC RTN network "The Physics of the Intergalactic Medium."

REFERENCES

Aguirre, A., Herquist, L., Schaye, J., Katz, N., Weinberg, D. H., & Gardiner, J. 2001a, ApJ, 561, 521
Aguirre, A., Herquist, L., Schaye, J., Weinberg, D. H., Katz, N., & Gardiner, J. 2001b, ApJ, 560, 599
Balbi, A., et al. 2000, ApJ, 545, L1
Bardeen, J. M., Bond, J. R., Kaiser, N., & Szalay, A. S. 1986, ApJ, 304, 15
Barkana, R. 2002, NewA, submitted (astro-ph/0201492)
Barkana, R., & Loeb, A. 1999, ApJ, 523, 54
Cen, R., & Bryan G. L. 2001, ApJ, 546, L81
Cen, R., & Ostriker J. P. 1999, ApJ, 519, L109
Ciardi, B., Ferrara, A., & Abel, T. 2000a, ApJ, 533, 594
Ciardi, B., Ferrara, A., Governato, F., & Jenkins, A. 2000b, MNRAS, 314, 611
Ellison, S. L., Songaila, A., Schaye, J., & Pettini, M. 2000, AJ, 120, 1175
Ferrara, A., Pettini, M., & Shchekinov, Y. 2000, MNRAS, 319, 539
Giavalisco, M., Steidel, C. C., Adelberger, K. L., Dickinson, M. E., Pettini, M., & Kellogg, M. 1998, ApJ, 503, 543
Gnedin, N. Y., & Ostriker J. P. 1997, ApJ, 486, 581
Hellsten, U., Dave, R., Hernquist, L., Weinberg, D. & Katz, N. 1997, ApJ, 487, 482
Ikeuchi, S., & Ostriker, J. P. 1986, ApJ, 301, 522
Kaiser, N. 1984, ApJ, 284, L9
Madau, P., Ferrara, A., & Rees, M. J. 2001, ApJ, 555, 92 (MFR01)
Makino, N., Sasaki, S., & Suto, Y. 1998, ApJ, 497, 555
Mori, M., Ferrara, A., & Madau P. 2002, ApJ, 571, 40 (MFM01)
Nagataki, S., & Sato, K. 1998, ApJ, 504, 629
Nath, B., & Chiba, M. 1995, ApJ, 454, 604
Navarro, J. F., Frenk, C. S., & White, S. D. M. 1997, ApJ, 490, 493 (NFW)
Netterfield, C. B., et al. 2001, ApJ, 571, 604
Oh, S. P. 2002, MNRAS, submitted (astro-ph/0201517)
Ostriker, J. B., & McKee, C. F. 1988, Rev. Mod. Phys., 60, 1
Pettini, M., Steidel, C. C., Adelberger, K. L., Dickinson, M., & Giavalisco, M. 2000, ApJ, 528, 96
Pryke, C., et al. 2002, ApJ, 568, 46
Rauch, M., Haehnelt, M. G., & Steinmetz, M. 1997, ApJ, 481, 601
Ricotti, M., Gnedin, N. Y., & Shull, J. M. 2000, ApJ, 534, 41
Scannapieco, E., & Broadhurst, T. 2001, ApJ, 549, 28 (SB01)
Scannapieco, E., Ferrara, A., & Broadhurst, T. 2000, ApJ, 536, L11
Scannapieco, E., Thacker, R. J., & Davis M. 2001, ApJ, 557, 605
Schaye, J., Rauch, M., Sargent, W. L. W., & Kim, T.-S. 2000, ApJ, 541, L1
Schneider, R., Ferrara, A., Natarajan, P., & Omukai, K. 2002a, ApJ, 571, 30
Schneider, R., Guetta, D., & Ferrara, A. 2002b, MNRAS, submitted (astro-ph/0201342)
Sheth, R. K., Mo, H. J., & Tormen, G. 2001, MNRAS, 323, 1
Somerville, R. S. 1997, Ph.D. thesis, Univ. California, Santa Cruz
Songaila, A. 2001, ApJ, 561, L153
Songaila, A., & Cowie, L. L. 1996, AJ, 112, 335
Sutherland, R. S., & Dopita, M. A. 1993, ApJS, 88, 253
Tegmark, M., Silk, J., & Evrard, A. 1993, ApJ, 417, 54
Thacker, R. J., Scannapieco, E., & Davis, M. 2002, ApJ, submitted (astro-ph/0205054)
Viana, P. T. P., & Liddle, A. 1996, MNRAS, 281, 323
Voit, G. M. 1996, ApJ, 465, 548
White, S. D. M., & Frenk, C. S. 1991, ApJ, 379, 52